# Energy Absorption of Gold Nanoshells in Hyperthermia Therapy

Changhong Liu, Chunting Chris Mi*, *Senior Member, IEEE*, and Ben Q. Li

***Abstract*—The unique optical characteristics of a gold nanoshell motivate the application of nanoshell-based hyperthermia in drug delivery and cancer treatment. However, most of our understanding on energy absorption and heat transfer is still focused on individual particles, which may not be accurate for nanoshell aggregates in a real application due to the strong optical interaction of nanoshells. This paper investigates the relationship between the optical interaction and the interparticle distance in the visible and near-infrared regions by means of a finite-difference time-domain (FDTD) method. The objective is to explore the energy transportation mechanism, which is critical for hyperthermia therapy. From the numerical simulation results of different forms of nanoshell aggregates, including individual nanoshells, 1-D chains, 2-D arrays, and 3-D clusters, it was found that the interparticle distance plays a crucial role from the maximal absorption point of view. The interparticle distance affects both field enhancement and surface plasmon resonance position. The accurate prediction of energy absorption also helps the way nanoshells are populated in the tumor cell so as to prevent heat damage to healthy tissues in clinic applications. In the case of 3-D clusters, the laser energy decays exponentially along the wave propagation, and the penetration depth greatly depends on the interparticle distance. The closer the nanoshells are placed, the shorter the penetration depth is. The maximal total length for the laser penetration through the shell of gold nanoparticles is about a few hundred to several nanometers. The actual penetration depth primarily depends not only on the interparticle distance, but also on the size of the nanoshells as well as other factors. Since the absorption energy is concentrated on the surface clusters of nanoparticles, heat transfer mechanisms in metal-nanoparticles-based hyperthermia will differ from that in other hyperthermia. The information obtained from this paper will serve as a basis for further study of heat transfer in metal-nanoparticles-based hyperthermia.**

***Index Terms*—Finite-difference time-domain (FDTD), hyperthermia, near-infrared (NIR) laser, surface plasmon resonance.**

## I. Introduction

WITH RECENT advances in material synthesis and fabrication, metal nanoshells composed of a dielectric core (for example, silica) coated with a thin noble metallic layer (for example, gold) have received considerable attention over the last decade. This is due to the unique optical, electric, and magnetic properties exhibited by the spherical particles at the nanoscale, which is not seen at bulk scale. For example, there is significant local electric field enhancement near the metal–dielectric interface due to the strong surface plasmon resonance (SPR) and the high tunability of the SPR frequency. It has been shown that for a gold nanoshell, the maximal field intensity in the vicinity of a nanoparticle is much larger than that of the incident field. Moreover, the SPR band can be widely tuned from the visible light (VIS) to the near-infrared (NIR) spectrum just by varying the ratio of shell thickness to the overall diameter of the particle [1]–[4]. These unique characteristics have found promising applications in a wide range of areas, such as biosensing, optical communication, astronomy, pharmaceuticals, and healthcare. One important application is for cancer treatment [5]–[7], known as nanoparticle-based hyperthermia. The principle for this application is that, when exposed to the appropriate wavelengths of a laser beam, the nanoshells pre-embedded in a tumor absorb energy, and then, heat up; yet, the healthy tissues along the laser path do not. With the increased temperature, cancerous cells gradually lose activity and die. The treatment at a temperature between 40 °C and 44 °C is cytotoxic for cells in an environment with hypoxia and low pH [8]–[10] conditions that are found to be largely associated with tumor tissue but not in normal tissues. This makes the nanoparticle-based hyperthermia superior to other traditional treatments for noninvasive and targeted therapy of cancer patients [11], [12].

The predominating benefit of nanoshell-based hyperthermia is that it is both safe and efficient. This is because most biological soft tissues have a relatively low light absorption coefficient in the VIS and NIR regions [13], [14], known as the tissue optical window or therapeutic window. Over this window, NIR light transmits through the tissues with scattering-limited attenuation and minimal heating. The healthy tissues are therefore prevented from the heat damage, which is inevitable in other thermal treatments, such as microwave and RF ablation [15], magnetic thermal ablation [16], and focused ultrasound therapy [17]. A combination of these two benign moieties (nanoshells and NIR light) allows a noninvasive delivery of heat to a tumor volume by using an extracorporeal, low-power diode laser to induce a photothermal destruction of the tumor embedded with nanoshell particles [18].

Thus far, the understanding of heat generation and heat transfer for nanoshell-enhanced hyperthermia studies has been based largely on the knowledge of the behavior of a single, isolated particle or a single nanostructure in an alternating electromagnetic field [19]–[23]. In a real process, however, a

Manuscript received October 14, 2007; revised February 17, 2008. Current version published August 29, 2008. This work was supported in part by the National Aeronautics and Space Administration (NASA) under Grant #: NAS 1477 and in part by the University of Michigan under the Office of the Vice President for Research (OVPR) Grant. *Asterisk indicates corresponding author.*

C. Liu is with Shanghai Jiao Tong University, Shanghai 200240 China, and also with the Department of Electrical and Computer Engineering, University of Michigan-Dearborn, Dearborn, MI 48128 USA (e-mail: lchsh@umd.umich.edu).

*C. C. Mi is with the Department of Electrical and Computer Engineering, University of Michigan-Dearborn, Dearborn, MI 48128 USA (e-mail: chrismi@umich.edu).

B. Q. Li is with the Department of Mechanical Engineering, University of Michigan-Dearborn, Dearborn, MI 48128 USA (e-mail: benqli@umich.edu).

Color versions of one or more of the figures in this paper are available online at http://ieeexplore.ieee.org.

Digital Object Identifier 10.1109/TNB.2008.2002284

great number of nanoparticles is needed to produce a thermal kill, and they may not be placed far away enough from each other in the tumor so that the analysis can be simplified as isolated individuals, especially in the light of the limitation associated with the current method by which these particles are injected into a tumor. Consequently, the absorption and scattering ability of nanoparticle aggregates should differ from that of an individual particle due to the strong optical and electromagnetic interaction of interparticles [24]–[29]. However, there appears to have been very little work, if not all, to study the interactive nature of nanoshell aggregates during the energy absorbing process. Such study is not only of critical importance to enhance the fundamental understanding of interparticle optical interference, but also essential to develop a hyperthermia technology with optimal thermal efficiency for cancer therapy.

The objective of this paper is to investigate the relationship of interparticle interactions and the interparticle distance in the VIS and NIR spectrum regions, and to understand the basic nature of the energy transport and absorption in nanoshell aggregates as a function of interparticle distance, particle size, and different forms of nanoshell collectives. Toward this end, the full-scale Maxwell equations are solved numerically using a finite-difference time-domain (FDTD) method. Systems studied include 1-D chains, 2-D arrays, and 3-D clusters. The information obtained from this study should shed light on the fundamental laws governing the energy absorption process in nanoparticles and will serve a basis for further study of heat transfer mechanisms associated with nanoshell aggregates.

It should be pointed out that since this paper is theoretical in nature, some assumptions were used to simplify the simulation model. First, the possibility of shape differences of nanoshells is ignored. Second, all the particles are assumed to be spherical shells and evenly distributed in spatial space.

## II. Research Methodology

The physical phenomenon of the interaction between metal particles and laser at optical frequencies can be described by macroscopic electromagnetic theory, namely, Maxwell's equations [30]. The analytical solution of Maxwell's equations of a single homogeneous sphere with an incident electromagnetic field was first given by Mie in 1908, which is the only simple, exact solution to Maxwell's equations that is relevant to particles. However, the analytical solution for the interaction problem is not always an easy job, especially for multiple objects with irregular geometry. In this case, numerical simulation provides good alternatives. Among many numerical techniques [31], the FDTD method [32]–[36] was chosen to study the light absorbing and scattering issues. Since the FDTD method is a time-domain approach, it is possible to obtain results for a full spectrum with a single simulation run. This is very important for SPR-associated problems, where resonant frequencies are not precisely known beforehand.

### A. Dispersive Material Models

Maxwell's equations in nonmagnetic materials are given by the following equations:

$$\frac{\partial \vec{D}}{\partial t} = \nabla \times \vec{H} \tag{1}$$

$$\vec{D}(\omega) = \varepsilon_0 \varepsilon_r^*(\omega)\vec{E}(\omega) \tag{2}$$

$$\frac{\partial \vec{H}}{\partial t} = -\frac{1}{\mu_0}\nabla \times \vec{E} \tag{3}$$

where $\vec{H}$, $\vec{E}$, and $\vec{D}$ represent the magnetic field vector, electric field vector, and electric displacement vector, respectively, $\omega = 2\pi f$ is the angular frequency; $\varepsilon_0$ and $\mu_0$ are permittivity and permeability of free space, respectively, and $\varepsilon_r^*(\omega)$ is the complex relative permittivity. It should be noted that the permittivity depends on both the frequency and particle size at optical frequency. This size effect can be ignored only when the geometry is larger than 10 nm [37].

In the time domain, (2) becomes a convolution:

$$\vec{D}(t) = \varepsilon_0 \varepsilon_r(t) * \vec{E}(t) = \int_{-\infty}^{+\infty} \vec{E}(\tau)\varepsilon(t-\tau)d\tau. \tag{4}$$

It is obvious that the electrical displacement vector $\vec{D}$ at time $t$ depends on the electrical field vector $\vec{E}$. Since it is difficult to calculate the convolution product directly, a dispersion model such as the Drude model, Lorentz model, plasma model, or Debye model [38] can be used to give an approximation. In this paper, a linear combination of the Lorentz model and plasma model [39] was employed to simulate the dispersive material. The total complex permittivity of the materials (gold) is given as (5), where each contribution arising from the different material models plays a role in the overall permittivity

$$\tilde{\varepsilon}(f) = \varepsilon_{\mathrm{REAL}} + \tilde{\varepsilon}_P(f) + \tilde{\varepsilon}_L(f) \tag{5}$$

where $\varepsilon_{\mathrm{REAL}}$ represents the contribution due to the basic, background permittivity, $\tilde{\varepsilon}_P(f)$ and $\tilde{\varepsilon}_L(f)$ represent the plasma and Lorentz contributions, respectively, which are defined as

$$\tilde{\varepsilon}_P(f) = -\frac{\omega_P^2}{2\pi f(i\nu_c + 2\pi f)} \tag{6}$$

$$\tilde{\varepsilon}_L(f) = -\frac{\varepsilon_{\mathrm{LORENTZ}}\omega_0^2}{(\omega_0^2 - 2i\delta_0 2\pi f - (2\pi f)^2)}. \tag{7}$$

The parameters in the previous models are adjusted to reproduce the experimental dielectric constant given by Johnson and Christy [39] within the frequency range of interest, where

$$\varepsilon_{\mathrm{REAL}} = 7.0765, \qquad \omega_P = 1.39 \times 10^{16}\ \mathrm{Hz}$$
$$\nu_c = 1.41 \times 10^{7}\ \mathrm{Hz}, \qquad \varepsilon_{\mathrm{LORENTZ}} = 2.323$$
$$\omega_0 = 4.63 \times 10^{15}\ \mathrm{Hz}, \qquad \delta_0 = 9.27 \times 10^{14}\ \mathrm{Hz}.$$

Fig. 1 shows a comparison between results from (4) and experimental data for gold in VIS and NIR regions. It can be seen that the result from the hybrid model matches the experimental data very well in the interested frequency region.

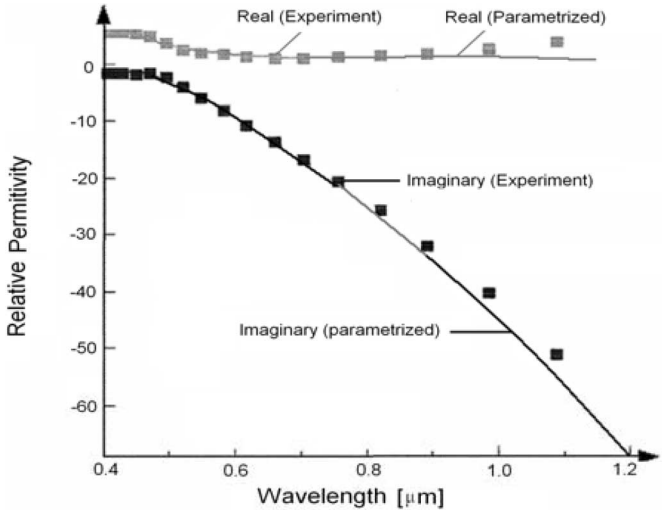


Fig. 1. Permittivity of gold in the VIS and NIR regions.

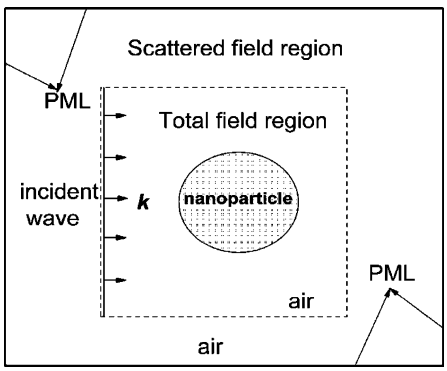


Fig. 2. Schematic of 2-D cross section of simulation domain.

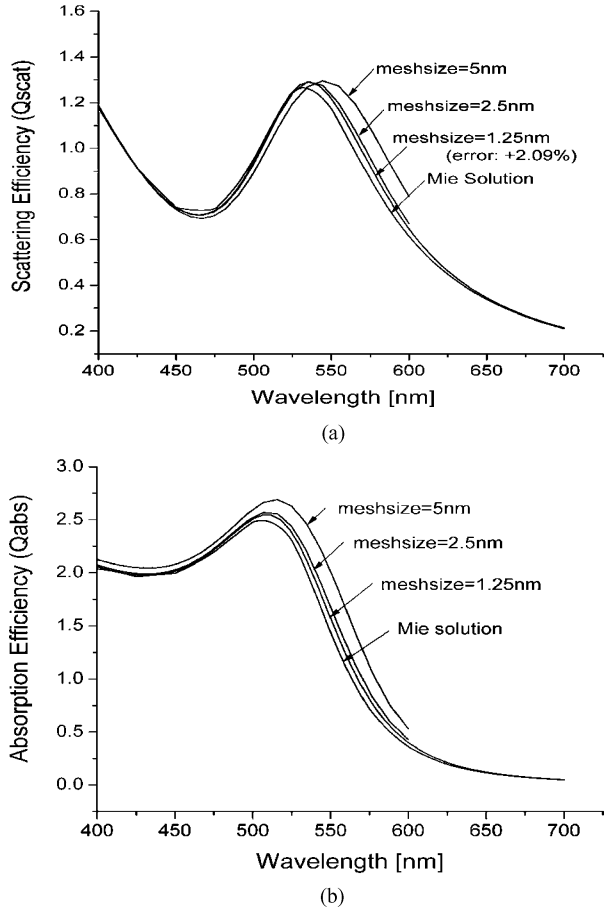


Fig. 3. Spectra of gold solid sphere with 100 nm diameter. The embedded medium is air. (a) Scattering efficiency. (b) Absorption efficiency.

### *B. Validation of FDTD Accuracy*

In order to examine the accuracy of the FDTD solution, a 3-D FDTD scattering model was built to be compared with the classical Mie's solution. The numerical simulation was performed by the FDTD Solutions software [40]. The model is a solid gold nanosphere with a diameter of 100 nm embedded in air, and the plane wave comes in from the left side, as shown in Fig. 2. The calculation region is truncated by six perfectly matched layers (PMLs) boundary. Since the FDTD technique uses a finite volume to consider the electromagnetic wave propagating in infinite space, e.g., simulate an open-region problem by using a closed one, the boundary condition must be able to absorb the scattered field component arriving at the boundary edge from all directions as if no artificial boundary is applied at all. Inside the PML surfaces, the electromagnetic field was divided into two regions: the total field region and the scattering field region. For nondissipative host media, by integrating in the two regions, the absorption energy and scattering energy by the gold nanosphere can be obtained as

$$W_{\text{scat}} = \frac{1}{2} R_e \left[ \iint_S (\vec{E}_{\text{scat}} \times \vec{H}^*_{\text{scat}}) \cdot \vec{n}\, ds \right] \quad (8)$$

$$W_{\text{abs}} = \frac{1}{2} R_e \left[ \iint_S (\vec{E}_{\text{tot}} \times \vec{H}^*_{\text{tot}}) \cdot \vec{n}\, ds \right] \quad (9)$$

where $\vec{E}_{\text{scat}}$ and $\vec{H}_{\text{scat}}$ are the scattering electric and magnetic field vectors, respectively, $\vec{E}_{\text{tot}}$ and $\vec{H}_{\text{tot}}$ are the total electric and magnetic field vectors, respectively, and $\vec{n}$ denotes the outward-pointing unit vector normal to the integration surface.

To exhibit the relative absorption and scattering ability of the gold nanosphere, the cross section and efficiencies for scattering and absorption can be defined as

$$C_{\text{abs}} = W_{\text{abs}}/I_{\text{inc}}, \quad C_{\text{scat}} = W_{\text{scat}}/I_{\text{inc}}, \quad C_{\text{ext}} = C_{\text{scat}} + C_{\text{abs}}$$

$$Q_{\text{abs}} = C_{\text{abs}}/A, \quad Q_{\text{scat}} = C_{\text{scat}}/A, \quad Q_{\text{ext}} = Q_{\text{scat}} + Q_{\text{abs}} \quad (10)$$

where $I_{\text{inc}} = (1/2)\varepsilon_0 c E^2$ represents the intensity of the incident wave, $A = \pi r^2$ is the particle cross-section area projected onto a plane perpendicular to the incident wave, and $r$ is the radius of the sphere.

Fig. 3 shows a comparison of the scattering efficiency and absorption efficiency obtained using the FDTD method and the classical Mie solution. As shown in Fig. 3, the difference between the numerical and analytical calculation depends on mesh size. This is because the field enhancement caused by SPR mainly focuses on the metal–dielectric interface and decays

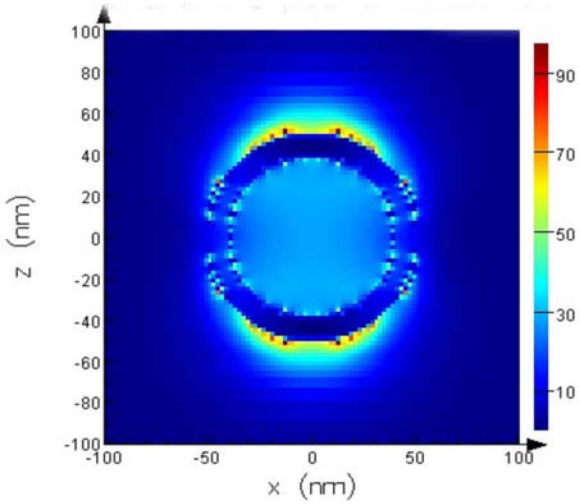


Fig. 4. Electric field enhancement for a gold nanoshell in water.

exponentially along the normal direction; therefore, the simulation is greatly sensitive to mesh conditions. To improve the results, the mesh size should be decreased as small as possible. For the case of a 100-nm-diameter gold nanosphere, good convergence has been achieved when the smallest element length is 1.25% of the diameter. The maximal magnitude difference to the Mie solution is +2.09%, and the resonance frequency for the Mie's solution occurs at 531.1198 nm, which appears at 535.98 nm for the FDTD simulation. Precision can be increased further; however, the simulation time increases significantly. In addition, our experience shows an average-wavelength span may be a better choice for the simulation region.

## III. Results and Discussions

### A. Geometry Effect of SPR

In hyperthermia therapy, if the SPR happens at an appropriate frequency range (for instance 700–1100 nm), where the absorption coefficient of healthy soft tissues is lower than that at any other frequencies, the surrounding tissues are expected to get minimal heat damage when light is delivered into the nanoparticles. Therefore, both safety and field enhancement can be obtained. Gold nanoshells are the primary choice of this strategy. Gold nanoshells exhibit strong scattering and absorption effects due to the SPR effect of the metallic–dielectric concentric spherical configuration.

Fig. 4 shows near-field enhancement by SPR of a gold shell embedded in water. The outer shell radius $R_1$ is 50 nm and the $SiO_2$ core radius $R_2$ is 40 nm. A P-polarized plane wave propagates along the $+x$-direction. At plasmon resonance frequency (wavelength is 699.057 nm), the maximal intensity is approximately 100 times the incident wave.

Fig. 5(a) shows that the optical resonance is a function of size and shape of the nanoparticles. Optical properties of gold nanoshells depend dramatically on the core-to-shell ratio. By varying the relative core and shell thickness, the maximal absorption energy and its position can be tuned across a broad range of the optical spectrum that spans the VIS light and the

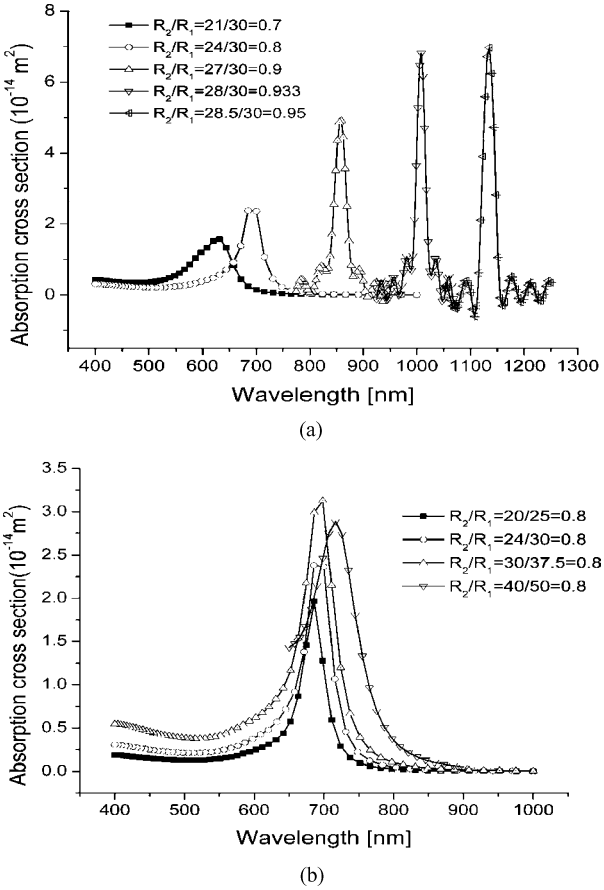


Fig. 5. Absorption cross section versus wavelength for gold nanoshell in water. (a) Outer shell radius is the same (30 nm), while thickness of the shell is different. From shorter to longer wavelength, the core-shell ratios are 0.7, 0.8, 0.9, 0.933, and 0.95, respectively. (b) Four nanoshells with the same core-to-shell ratio of 0.8 but different radii.

NIR spectral regions. The larger the core-to-shell ratio, the further the resonance frequency shifts into the infrared region. In Fig. 5(b), four groups of gold nanoshells were compared in terms of the ability of absorption energy. The outer radius of the nanoshells is from 25 to 50 nm, and shell thickness is from 5 to 10 nm. Although the nanoshells vary in size, they have the same core-to-shell ratio (i.e., 0.8). The curves reveal that under the same ratio, nanoshell size contributes only to the relative magnitude of absorption cross section and does not affect the resonance frequency location. It should be noted that since the surrounding medium (biological soft tissues) is almost transparent at the wavelengths considered here, only the absorption of the laser light by the particles is calculated.

### B. Interparticle Distance and Energy Absorption

*1) Triplet Chain:* Although a single particle is of prime interest for fundamental research, it is not sufficient for practical application. When particles aggregate, the optical properties of the nanoparticle assemblies are highly dependent on the separation between neighboring particles due to the strong dipole–dipole interaction. Some computed spectra are shown in Fig. 6 for triplet aggregates of gold nanoshells in water with inner

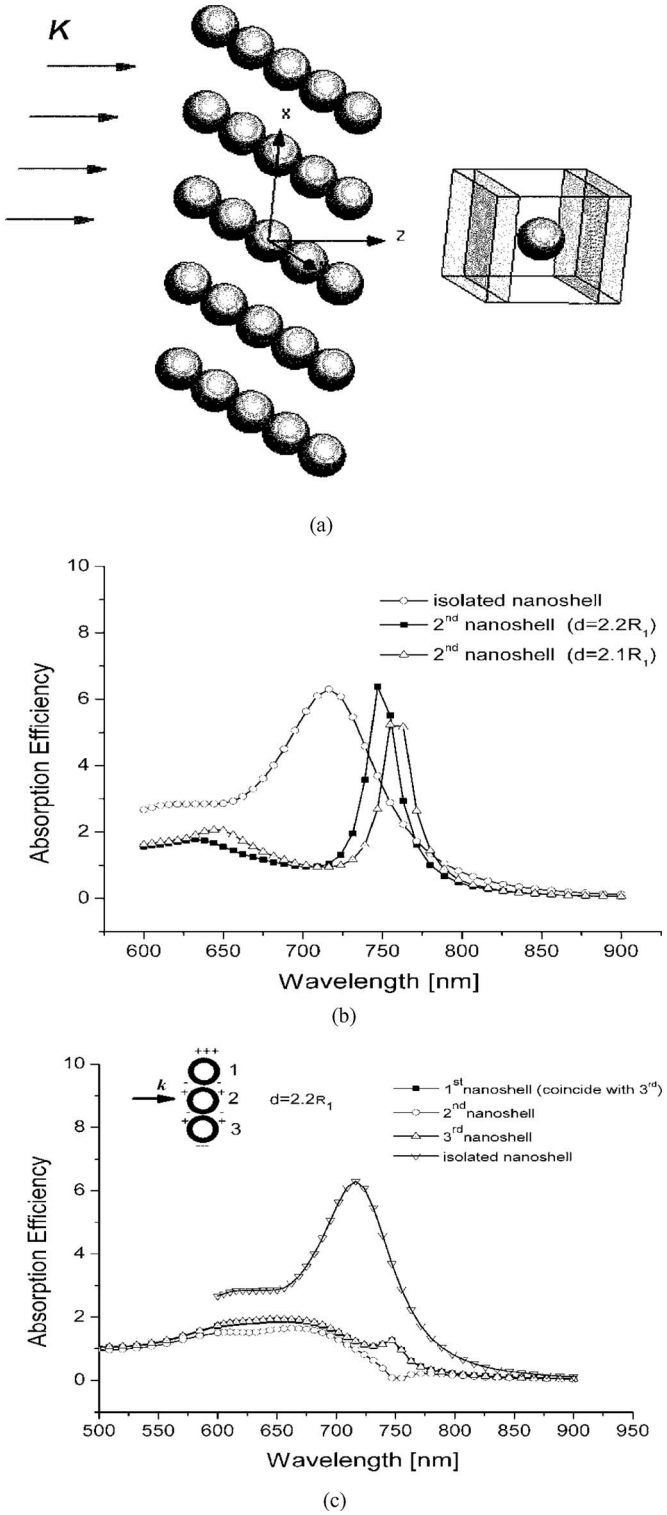


Fig. 6. Nanoshells interaction. (a) Triplet aggregates parallel to the wave vector. (b) Interparticle distance effect. (c) Triplet aggregates perpendicular to the wave vector.

and outer diameters of 40 and 50 nm, respectively. When the triplet aggregates were placed along the wave propagation direction (denoted by vector $\boldsymbol{k}$), as shown in Fig. 6(a), dipole coupling makes the SPR slightly red shifted. For example, the SPR is at $\lambda = 713.33$ nm for the isolated nanoshell. When three nanoshells are placed together, the SPR becomes 738.94, 746.81, and 754.84 nm from the first nanoshell to the third nanoshell, respectively. The SPR shift also depends on the interparticle distance, which can be seen from Fig. 6(b). When the distance $d$ decreased from $2.2R_1$ to $2.1R_1$, the SPR of the middle nanoshell shifted approximately 10 nm toward the infrared spectrum. Fig. 6(c) depicts the case of the triplet axis perpendicular to vector $\boldsymbol{k}$. Hence, the absorption efficiency was significantly decreased when three nanoshells are placed closer to each other (e.g., $d = 2.2R_1$). Also in this case, there was a blue shift for SPR position.

The optical properties of nanoshell collectives, whose size is much smaller than the wavelength, finally owe to the interactions of the dipoles of the nanoshell assemblies. The total electric field generated by the parallel triplets in Fig. 6(a) obviously differs from the perpendicular one in Fig. 6(c). In addition, it is not difficult to imagine that the dipoles coupling should also be a function of the interparticle distance. If the separation between the nanoshells were long enough, the interaction can be ignored in near field accordingly.

*2) Nanoshell Array:* In order to further investigate the effect of distance, models of nanoshell arrays with different interparticle distances were studied, as shown in Fig. 7(a), where the incident plane wave propagates along the $z$-direction, and the nanoshells were evenly placed in the $x$–$y$ plane. This can be regarded as the extension of the vertical triplet chain in Fig. 6(c), where the nanoshell number is assumed infinite in the $x$- and $y$-directions. In this case, the truncated boundaries parallel to the wave vector may be treated as a periodic boundary condition. Note that the boundaries vertical to the wave vector still satisfy the PML condition. Fig. 7(b) and (c) describes the maximal absorption efficiency as a function of the interparticle distance for nanoshells with inner and outer diameter of 40 and 50 nm in air, and those with inner and outer diameter of 28 and 30 nm in water.

When the nanoshell array is vertical to the incident wave, there is a specific distance corresponding to the maximal absorption, although the size of the nanoshell and the surrounding medium is different. From the maximal energy absorption point of view, the distance makes no difference to the maximal energy absorption. It is believed that this is because of the combined effects of the relative size to the wavelength and the interparticle distance. The former determines the type of interaction (distribution of electrons and modes of resonance), and the latter determines the degree of interactions. An optimum combination may lead to high-field enhancement. Furthermore, it is noticed that when the distance between the particles is long enough (e.g., $200R_1$), the peak height and peak height position of absorption power of any particle behaves the same as those of an isolated particle. This is because the influence between any two particles becomes weak in the near field as the distance increases. To some extent, this validates the effectiveness of the simulation model.

*3) Nanoshell Clusters:* When nanoshells distribute in 3-D space evenly, it may be regarded as many layers of 2-D arrays spreading along the $z$-direction. Although periodic boundary conditions can be employed to describe the infinity nanoshells parallel to the wave vector, equivalent boundary conditions for

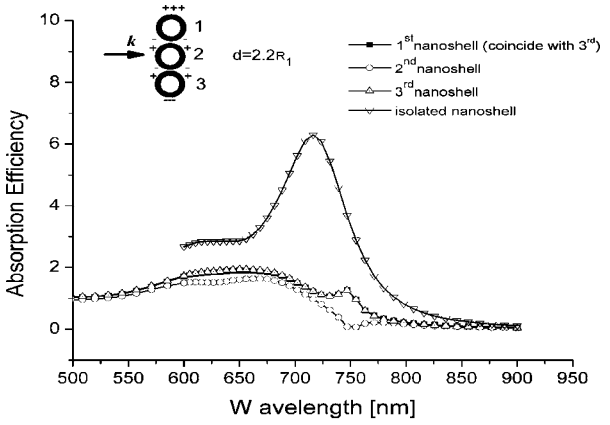


(a)

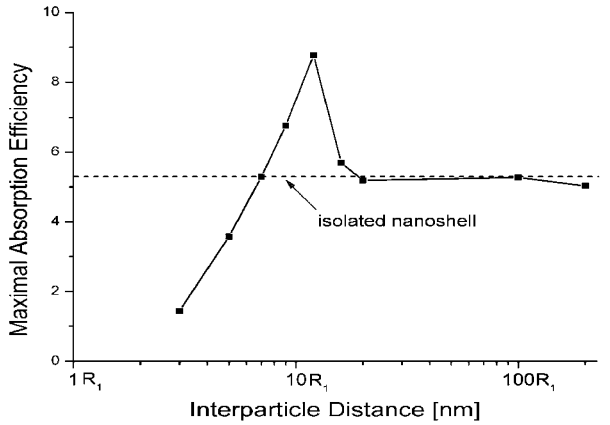


(b)

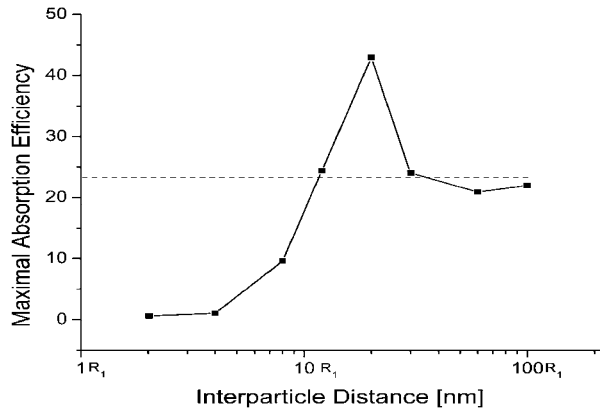


(c)

Fig. 7. Distance effect of lattice of nanoshells. (a) Simulation model in FDTD. (b) Maximal absorption efficiency versus interparticle distance for gold nanoshells in air, whose size is (40 nm, 50 nm). (c) Maximal absorption efficiency versus distance for gold nanoshells in water, whose size is (40 nm, 50 nm).

direct numerical simulation of nanoshells along the wave vector is still impractical due to the attenuation of electromagnetic field with wave propagation. Therefore, the model including as many layers as possible was employed here. A cross-section schematic drawing is shown in Fig. 8(a). The two surfaces perpendicular to $\boldsymbol{k}$ still satisfy the PML boundary condition while the other four surfaces parallel to $\boldsymbol{k}$ satisfy the periodic boundary condition (PBC). The computational model includes seven-layer

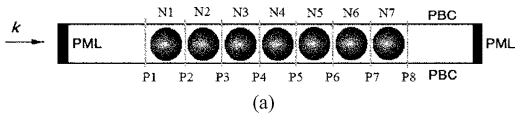


(a)

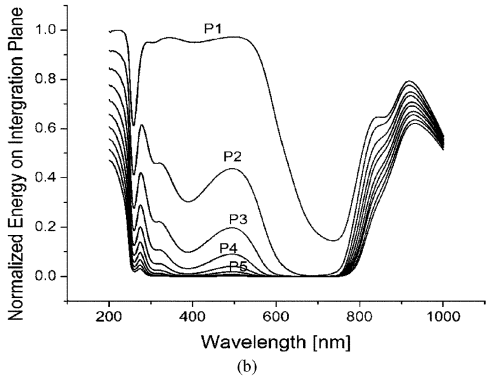


(b)

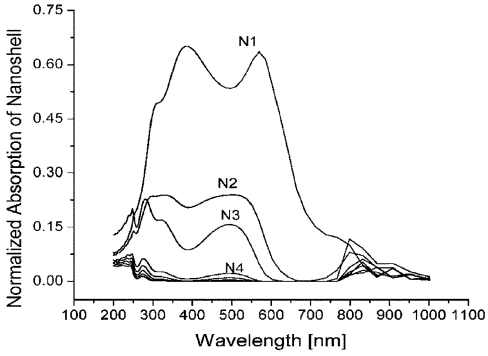


(c)

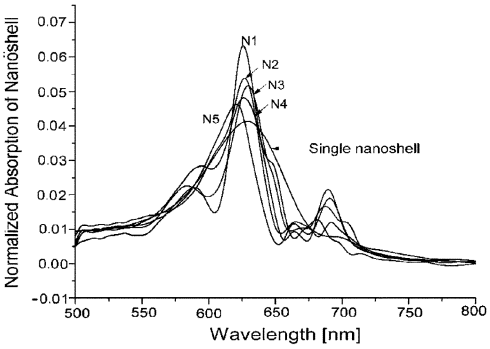


(d)

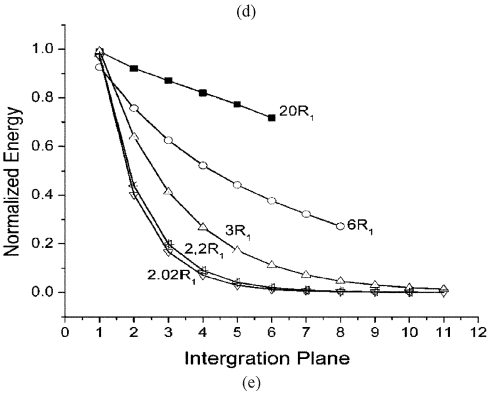


(e)

Fig. 8. Nanoshell cluster model and absorption energy results. (a) 2-D cross-section schematic of model. (b) Normalized energy on the eight integration planes, where gold nanoshell is (40 nm, 50 nm) $d = 2.2R_1$ and seven layers are included in the model. (c) Normalized energy absorbed by the seven nanoshells corresponding to (b). (d) Normalized energy absorbed by nanoshells, where $d = 20R_1$, five layers included. (e) Energy attenuation varying with the interparticle distance, where the horizontal coordinate is the integration plane number.

nanoshells and eight energy integration planes, numbered $N1$–$N7$ and $P1$ to $P7$ from left to right, respectively. The energy difference between any two adjacent planes will be the energy absorbed by the nanoshell.

The energy distribution in the eight integration planes versus wavelength and the energy absorbed by the nanoshells were given in Fig. 8(b) and (c), where the (40 nm, 50 nm) gold nanoshells placed in air were considered, and the interparticle distance is $d = 2.2R_1$. Fig. 8(d) is the energy absorbed by the nanoshells when d increased to $20R_1$. Fig. 8(e) is the energy attenuation with laser propagation versus interparticle distance.

For a single nanoshell with inner and outer diameters of 40 and 50 nm embedded in air, the SPR position happens at 632.258 nm. Therefore, the discrepancy for the region where the wavelength is longer than 650 nm is caused by a numerical error, as shown in Fig. 8(c) and (d). In the simulation of multiple nanoparticles, the smallest mesh size is increased to 2.5% of the diameter to save the calculation time. It can be seen from Fig. 8 that when nanoshells get closer to each other (e.g., $2.2R_1$), the general SPR appears slightly blue shifted compared to the isolated case. Furthermore, some of the waveforms of SPR have double peaks. This is because with incident wave propagation, more and more particles contribute to the total electromagnetic field, which, in turn, leads to the high-order coupling to gradually become the dominant contribution. For the first particle, the contribution of the dipole and quadruple is almost the same, but for the third one, the quadruple coupling is dominant. For the fourth and the following particles, the coupling is of higher order. This means that if the interparticle distance is small, not all the particles reach the peak absorption condition under the same frequency. The SPR position of the particles far from the incident side tends to be blue shifted. Fig. 8(d) shows the case with a long interparticle distance ($20R_1$). It can be seen that both the SPR position and absorption magnitude of multiple particles are close to those of an individual particle. This is reasonable since the interaction is very weak at a long interparticle interval. Besides the earlier two special cases (small distance and long distance), the other four interparticle distances were also considered in this paper.

Taking the normalized energy of all the integral planes at the wavelength corresponding to the maximal absorption for the first nanoparticles, the curves were obtained for the energy decay in gold nanoshells varying with interparticle distance, as shown in Fig. 8(e). It can be seen that the energy decays exponentially while the laser is delivered into the nanoshells. The attenuation depends on the separation space of the nanoshells: the closer the interparticle distance, the fewer layers the incident wave can penetrate through. For instance, when $d = 20R_1$ (or $d = 1000$ nm), under which the particles interaction is assumed to be weak, the incident laser penetrates approximately 15 layers of particles. For layers with a thickness of 20 nm, the maximal thickness of a gold shell that the laser penetrates is around 300 nm. However, when $d = 2.02R_1$ (or $d = 101$ nm), the electromagnetic wave penetrates less than two layers (<40 nm) when the energy input decays to $1/e$.

In order to further validate the previous conclusion, cases for smaller gold nanoshells in water, with $R_2 = 28$ nm and $R_1 = 30$ nm, were simulated. The results are shown in Fig. 9.

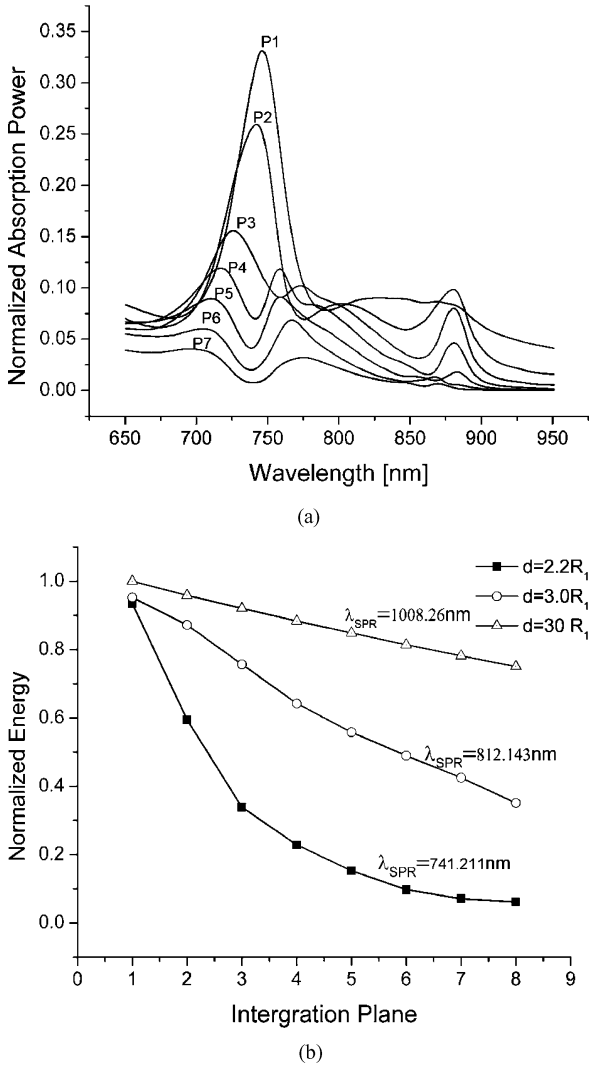


Fig. 9. Absorption energy results of (28 nm, 30 nm) nanoshell clusters in water. (a) Normalized energy absorbed by the seven nanoshells with $d = 2.2R_1$. (b) Energy attenuation versus interparticle distance.

For an individual (28 nm, 30 nm) nanoshell in water, the position of SPR caused by dipole coupling is 1008.26 nm. For the multiparticles with interparticle distance at $2.2R_1$, the positions of SPR for the nanoparticles obviously move toward the blue light spectrum. Moreover, the coupling order increases with wave propagation. In Fig. 9(b), the penetration depth is still distance-dependent. The maximal penetration depth is 24 layers (96 nm) at the distance of $30R_1$, where interparticle interactions are believed weak enough to be ignored. When the distance is $2.2R_1$, the penetration depth is only two layers (8 nm).

Although a general expression describing the penetration depth as a function of particle size, type of aggregates, material properties, interparticle distances, and working frequency is not available now, it has been found in this study that the energy transfer mechanism of gold nanoshells in the NIR region is different from that in bulk material, where the penetration depth is believed to be 30–40 nm in the NIR region [37]. The earlier results show that the penetration depth is several nanometers to several hundred nanometers. This means that the heat transfer

by nanoparticles might be more important than the energy absorption toward the depth of the tumor. It is shown that with more particles populated inside the tumor, the particles toward the inside of the tumor do not help to generate more heat in the target area. But the nanoparticles may help in the heat transfer from the surface area to the inside of the tumor due to the good heat conductivity of the nanoshells. Only the several surface layers of nanoparticles absorb heat if high-concentration nanoshells were used. Due to this fact, the heat analysis based on average heat source may bring significant discrepancy from the true situation.

## IV. Conclusion

The optical properties of gold nanoshell aggregates in the VIS and NIR spectrum were studied by means of the FDTD method. First, the classical Mie's solution for a gold solid nanosphere was obtained to validate the accuracy of FDTD. Results show that the FDTD simulation agrees very well with the analytical results when the mesh size is reasonably assigned. On this basis, electromagnetic wave diffusion in gold nanoshells was analyzed for isolated particles, 1-D chains, 2-D arrays, and 3-D clusters, respectively. The following conclusions are obtained from this study.

1) Optical properties of gold nanoshells depend dramatically on the core-to-shell ratio. For the same core-to-shell ratio, the SPR position appears at the same wavelength. For the same outer shell diameter, the maximal absorption power and SPR position can be tuned across a broad range of the optical spectrum that spans the VIS and the NIR spectral regions. The bigger the core-to-shell ratio, the longer the SPR wavelength.
2) The SPR peak height and position of a gold nanoshell chain depend on both the interparticle distance and wave direction. When the wave vector is parallel to the chain, SPR is slightly red shifted. When the wave vector is perpendicular to the chain, SPR is blue shifted.
3) In the case of a 2-D array, the absorption energy by the nanoshells relies on the interparticle distance. There is an optimum distance for a given particle size.
4) In the case of 3-D evenly distributed nanoshell clusters, the SPR position shifted toward shorter wavelength in comparison to the SPR position of an isolated particle. As a result, the core-to-shell ratio of nanoshells in real applications should be greater than the results obtained from the single nanoshell analysis, which may help the SPR to occur in the "tissue window" region.

In the VIS and NIR regions, the penetration depth of the electromagnetic wave in 3-D nanoshell clusters is inversely proportional to the interparticle distance (or concentration). For the nanoshells with radius (28 nm, 30 nm) in water, the maximal penetration depth is about 15 layers when the interparticle distance $d$ is large such that the interference may be ignored. When $d$ is very small, the laser can only penetrate less than two to three layers. This means that only a few surface layers of nanoshells embedded in the tumor area absorb heat in hyperthermia treatment. As a result, other nanoshells may only transfer heat. The optimum interparticle distance (or concentration) should be determined by combining electromagnetic and heat transfer theory. This will be our future paper.

## Acknowledgment

The authors would like to thank Lumerical Solutions, Inc., who supplied the academic licenses of their FDTD solution software for this study.

## References

[1] J. B. Jackson, S. L. Westcott, L. R. Hirsch, J. L. West, and N. J. Halas, "Surface enhanced Raman effect via the nanoshell geometry," *Appl. Phys. Lett.*, vol. 82, pp. 257–259, 2003.
[2] H. S. Zhou, I. Honma, and H. Komiyama, "Controlled synthesis and quantum-size effect in gold-coated nanoparticles," *Phys. Rev. B.*, vol. 50, pp. 12052–12056, 1994.
[3] S. J. Oldenburg, S. L. Westcott, R. D. Averitt, and N. J. Halas, "Surface enhanced Raman scattering in the near infrared using metal nanoshell substrates," *J. Chem. Phys.*, vol. 111, no. 10, pp. 4729–4735, 1999.
[4] L. R. Hirsch, A. M. Gobin, A. R. Lowery, F. Tam, R. A. Drezek, N. J. Halas, and J. L. West, "Metal nanoshells," *Ann. Biomed. Eng.*, vol. 34, no. 1, pp. 15–22, 2006.
[5] A. W. H. Lin, N. J. Halas, and R. A. Drezek, "Optically tunable nanoparticle contrast agents for early cancer detection: Model-based analysis of gold nanoshells," *J. Biomed. Opt.*, vol. 10, pp. 064035-1–064035-10, 2005.
[6] B. Klebtsov, V. Zharov, A. Melnikov, V. Tuchin, and N. Khlebtsov, "Optical amplification of photothermal therapy with gold nanoparticles and nanoclusters," *Nanotechnology*, vol. 17, pp. 5167–5179, 2006.
[7] M. Everts, J. L. Leddon, R. J. Kok, M. A. Preuss, C. L. Millican, D. E. Nikles, D. T. Johnson, and D. T. Curiel, "Gold nanoparticles as an amplifying payload strategy for adenoviral cancer gene therapy," *Nano Lett.*, vol. 6, no. 4, pp. 587–591, 2006.
[8] J. L. West and N. J. Halas, "Applications of nanotechnology to biotechnology," *Curr. Opin. Biotechnol.*, vol. 11, pp. 215–217, 2000.
[9] C. Loo, A. Lin, L. Hirsch, M.-H. Lee, J. Barton, N. Halas, J. West, and R. Drezek, "Nanoshell-enabled photonics-based imaging and therapy of cancer," *Technol. Cancer Res. Treat.*, vol. 3, no. 1, pp. 33–40, 2004.
[10] D. Rotin, B. Robinson, and I. F. Tannock, "Influence of hypoxia and an acidic environment on the metabolism and viability of cultured cells," *Cancer Res.*, vol. 46, pp. 2821–2826, 1986.
[11] E. Helm, "Nanotechnology may replace existing treatments for cancer," *Eukaryon*, vol. 3, p. 55, 2007.
[12] N. W. S. Kam, M. O'Connell, J. A. Wisdom, and H. Dai, "Carbon nanotubes as multifunctional biological transporters and near-infrared agents for selective cancer cell destruction," *Proc. Natl. Acad. Sci.*, vol. 102, no. 33, pp. 11600–11605, 2005.
[13] J. P. Ritz, A. Roggan, C. Isbert, G. Müller, H. J. Buhr, and C. T. Germer, "Optical properties of native and coagulated porcine liver tissue between 400 and 2400 nm," *Lasers Surg. Med.*, vol. 29, pp. 205–212, 2001.
[14] A. N. Yaroslavsky, P. C. Schulze, I. V. Yaroslavsky, R. Schober, F. Ulrich, and H. J. Schwarzmaier, "Optical properties of selected native and coagulated human brain tissues *in vitro* in the visible and near infrared spectral range," *Phys. Med. Biol.*, vol. 47, pp. 2059–2073, 2002.
[15] G. S. Gazelle, S. N. Goldberg, L. Solbiati, and T. Livraghi, "Tumor ablation with radio-frequency energy," *Radiology*, vol. 217, no. 3, pp. 633–646, 2000.
[16] I. Hilger, W. Andra, R. Bahring, A. Daum, R. Hergt, and W. A. Kaiser, "Evaluation of temperature increase with different amounts of magnetite in liver tissue samples," *Invest. Radiol.*, vol. 32, no. 11, pp. 705–712, 1997.
[17] F. A. Jolesz and K. Hynynen, "Magnetic resonance image-guided focused ultrasound surgery," *Cancer J.*, vol. 8, pp. S100–S112, 2002.
[18] L. R. Hirsch, R. J. Stafford, J. A. Bankson, S. R. Sershen, B. Rivera, R. E. Price, J. D. Hazle, N. J. Halas, and J. L. West, "Nanoshell-mediated near-infrared thermal therapy of tumors under magnetic resonance guidance," *Proc. Natl. Acad. Sci.*, vol. 100, no. 23, pp. 13549–13554, 2003.
[19] R. D. Averitt, S. L. Westcott, and N. J. Halas, "Linear optical properties of gold nanoshells," *J. Opt. Soc. Am. B*, vol. 16, no. 10, pp. 1824–1832, 1999.
[20] A. Lin, N. A. Lewinski, M. H. Lee, and R. A. Drezek, "Reflectance spectroscopy of gold nanoshells: computational predictions and experimental measurements," *J. Nanoparticle Res.*, vol. 8, pp. 681–692, 2006.

[21] M. Alam and Y. Massoud, "A closed-form analytical models for single nanoshells," *IEEE Trans. Nanotechnol.*, vol. 5, no. 3, pp. 265–272, May 2006.
[22] N. Harris, M. J. Ford, and M. B. Cortie, "Optimization of plasmonic heating by gold nanospheres and nanoshells," *J. Phys. Chem. B.*, vol. 110, pp. 10701–10707, 2006.
[23] V. K. Pustovalov, "Theoretical study of the heating of solid ellipsoidal nanoparticle in media by short laser pulses," *Laser Phys. Lett.*, vol. 2, no. 8, pp. 401–406.
[24] B. Lamprecht, G. Schider, R. T. Lechner, H. Ditlbacher, J. R. Krenn, A. Leitner, and F. R. Aussenegg, "Metal nanoparticle ratings: Influence of dipolar particle interaction on the plasmon resonance," *Phys. Rev. Lett.*, vol. 84, no. 10, pp. 4721–4724, 2000.
[25] L. A. Sweatlock, S. A. Maier, and H. A. Atwater, "Highly confined electromagnetic fields in arrays of strongly coupled Ag nanoparticles," *Phys. Rev. B.*, vol. 71, pp. 235408-1–235408-7, 2005.
[26] M. L. Brongersma and P. G. Kik, *Surface Plasmon Nanophotonics*, M. L. Brongersma and G. Pieter, Eds. Berlin, Germany: Springer-Verlag, 2007.
[27] B. Khlebtsov, V. Zharov, A. Melnikov, V. Tuchin, and N. Khlebtsov, "Optical amplification of photothermal therapy with gold nanoparticles and nanoclusters," *Nanotechnology*, vol. 17, pp. 5167–5179, 2006.
[28] Z. Liu, H. Wang, H. Li, and X. Wang, "Red shift of plasmon resonance frequency due to the interacting Ag nanoparticles embedded in single crystal $SiO_2$ by implantation," *Appl. Phys. Lett.*, vol. 72, pp. 1823–1825, 1998.
[29] W. M. Saj, T. J. Antosiewicz, J. Pniewski, and T. Szoplik, "Energy transport in plasmon waveguide on chains of nanoplates," *Optoelectronics Rev.*, vol. 14, no. 3, pp. 243–251, 2006.
[30] G. W. Ford and W. H. Weber, "Electromagnetic interactions of molecules with metal surfaces," *Phys. Rep.*, vol. 113, no. 4, pp. 195–287, 1984.
[31] F. M. Kahnert, "Numerical methods in electromagnetic scattering theory," *J. Quant. Spectrosc. Radiat. Transfer*, vol. 79/80, no. 1, pp. 775–824, Sep. 2003.
[32] K. S. Kunz and R. J. Luebbers, *The Finite Difference Time Domain Method for Electromagnetics*. Boca Raton, FL: CRC Press, 1993.
[33] A. Taflove and S. C. Hagness, *Computational Electrodynamics: The Finite-Difference Time-Domain Method*, 2nd ed. Norwood, MA: Artech House, 2000.
[34] S. Tanev, V. V. Tuchin, and P. Paddon, "Light scattering effects of gold nanoparticles in cells: FDTD modeling," *Laser Phys. Lett.*, vol. 3, no. 12, pp. 594–598, 2006.
[35] C. Oubre and P. Nordlander, "Optical properties of metallic dielectric nanostructures calculated using the finite difference time domain method," *J. Phys. Chem. B*, vol. 108, pp. 17740–17747, 2004.
[36] C. Oubre and P. Nordlander, "Finite difference time domain studies of the optical properties of nanoshell dimers," *J. Phys. Chem. B*, vol. 109, pp. 10042–10051, 2005.
[37] U. Kreibig and M. Vollmer, *Optical Properties of Metal Clusters* (Springer Series in Materials Science 25). New York: Springer-Verlag, 1995.
[38] C. F. Bohren and D. R. Huffman, *Absorption and Scattering of Light by Small Particles*. New York: Wiley, 1983.
[39] P. B. Johnson and R. W. Christy, "Optical constants of the noble metals," *Phys. Rev. B*, vol. 6, pp. 4370–4379, 1972.
[40] *The FDTD Solutions*™. (2007). Lumerical Solutions, Inc., Vancouver, BC, Canada. [Online]. Available: www.lumerical.com

**Changhong Liu** received the B.S. degree in electrical engineering from Hefei University of Technology, Hefei, China, in 1992, and the M.S. degree from Tsinghua University, Beijing, China, in 2001. She is currently working toward the Ph.D. degree at Shanghai Jiao Tong University, Shanghai, China.

Since 2001, she has been a Lecturer at Shanghai Jiao Tong University. She is also a Research Scholar at University of Michigan-Dearborn, Dearborn. Her current research interests include electromagnetic field, heat transfer, and cooling technology.

**Chunting Chris Mi** (S'00–A'01–M'01–SM'03) received the B.S.E.E. and M.S.E.E. degrees from the Northwestern Polytechnical University, Xi'an, China, and the Ph.D. degree from the University of Toronto, Toronto, ON, Canada, all in electrical engineering.

From 2000 to 2001, he was an Electrical Engineer with General Electric Canada, Inc., where he was engaged in designing and developing large electric motors and generators up to 30 MW. He was at the Rare-Earth Permanent Magnet Machine Institute, Northwestern Polytechnical University. In 1994, he joined Xi'an Petroleum Institute as an Associate Professor and an Associate Chair of the Department of Automation. From 1996 to 1997, he was a visiting scientist at the University of Toronto. He is currently an Associate Professor and the Director of the Data Terminal Equipment (DTE) Power Electronics and Electrical Drives Laboratory, Department of Electrical and Computer Engineering, University of Michigan-Dearborn, Dearborn. He is the author or coauthor of more than 80 articles on the subject of electric machines, power electronics, and electric and hybrid vehicles. His current research interests include electric drives, power electronics, electric machines, renewable energy systems, and electrical and hybrid vehicles.

Dr. Mi is the Chair of the IEEE Southeastern Michigan Section (2008–2009). He was the Vice Chair of the Section from 2006 to 2007. He is the recipient of the "National Innovation Award," the "Government Special Allowance Award," and the "Distinguished Teaching Award" of the University of Michigan-Dearborn. He is also the recipient of the 2007 IEEE Region 4 "Outstanding Engineer Award," the "IEEE Southeastern Michigan Section Outstanding Professional Award," and the "Society of Automotive Engineers (SAE) Environmental Excellence in Transportation (E2T) Award."

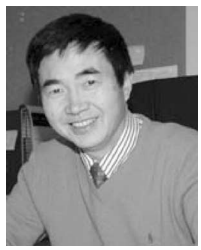

**Ben Q. Li** received the B.S. degree in 1982 from the Central University, Hunan, China, the M.S. degree in 1984 from Colorado School of Mines, Golden, and the Ph.D. degree in 1989 from the University of California, Berkeley, all in mechanical engineering.

He was a Research Associate at Massachusetts Institute of Technology for about a year, and a Senior Engineer at Aluminum Company of America (Alcoa) for three years. He is currently a Professor and the Chair of the Department of Mechanical Engineering, University of Michigan-Dearborn, Dearborn. He has authored one book and edited two books. He is also the author or coauthor of more than 200 technical papers in archive journals and conference proceedings. He has been an invited keynote speaker at many domestic and international conferences. His research work has been supported by various federal [National Science Foundation (NSF), National Aeronautics and Space Administration (NASA), Department of Energy (DOE), Department of Defense (DOD), the National Institute of Standards and Technology (NIST)] and state agencies as well as private industries. His current research interests include the study of electromagnetics, fluid flow, and heat transfer in thermal-fluid systems.

Prof. Li is a Fellow of the American Society for Mechanical Engineers.